Radiation Physics and Chemistry 130 (2017) 186–195

Contents lists available at ScienceDirect

Radiation Physics and Chemistry

journal homepage: www.elsevier.com/locate/radphyschem

Monte Carlo simulation of random, porous (foam) structures for neutron detection

Michael A. Reichenberger*, Ryan G. Fronk, J. Kenneth Shultis, Jeremy A. Roberts, Nathaniel S. Edwards, Sarah R. Stevenson, Christopher N. Tiner, Douglas S. McGregor

S.M.A.R.T. Laboratory, Mechanical and Nuclear Engineering Dept., Kansas State University, Manhattan KS 66506, USA

HIGHLIGHTS

- Description and testing of novel Dynamic Path Generation Monte Carlo technique.
- Characterization of the physical structure of RVC foams with various porosities.
- Preliminary validation of Dynamic Path Generation by comparison to MCNP6.
- Optimization study of simulated B_4C-coated RVC foam materials.

ARTICLE INFO

Article history:
Received 5 January 2016
Received in revised form
22 August 2016
Accepted 27 August 2016

Keywords:
Monte Carlo
Neutron detection
RVC foam
Boron-carbide
Lithium-fluoride

ABSTRACT

Porous media incorporating highly neutron-sensitive materials are of interest for use in the development of neutron detectors. Previous studies have shown experimentally the feasibility of ^{6}LiF-saturated, multi-layered detectors; however, the random geometry of porous materials has limited the effectiveness of simulation efforts. The results of scatterless neutron transport and subsequent charged reaction product ion energy deposition are reported here using a novel Monte Carlo method and compared to results obtained by MCNP6. This new Dynamic Path Generation (DPG) Monte Carlo method was developed in order to overcome the complexities of modeling a random porous geometry in MCNP6. The DPG method is then applied to determine the optimal coating thickness for $^{10}B_4C$-coated reticulated vitreous-carbon (RVC) foams. The optimal coating thickness for 4.1275 cm-thick $^{10}B_4C$-coated reticulated vitreous carbon foams with porosities of 5, 10, 20, 30, 45, and 80 pores per inch (PPI) were determined for ionizing gas pressures of 1.0 and 2.8 atm. A simulated, maximum, intrinsic thermal-neutron detection efficiency of $62.8 \pm 0.25\%$ was predicted for an 80 PPI RVC foam with a 0.2 μm thick coating of $^{10}B_4C$, for a lower level discriminator setting of 75 keV and an argon pressure of 2.8 atm.

1. Research motivation

Porous materials are currently under investigation for use as thermal-neutron detectors. Highly neutron-absorbing materials that react with thermal neutrons and produce energetic ions as reaction products must be incorporated in the porous material to enable the detection of neutrons. The charged-particle reaction products ionize gas within the pores of and surrounding the porous material. This ionization is then collected at the detector electrodes to produce an electronic pulse that records the neutron interaction event (Tsoulfanidis, 1995). Typically, ^{10}B or ^{6}Li are incorporated into the porous material either by impregnation or as a coating (Nelson et al., 2012).

Porous materials consist of struts and pores. Struts provide the structural support for the porous material and are composed of solid material which connect to form the support network. Pores consist of the void between struts in a porous material, and in the case of open-cell materials, are filled by any fluid within which the porous material is immersed. A generic example of a porous material is shown in Fig. 1. The original bubbles that exist during the manufacture of the porous material form a perfectly-packed, three-dimensional array of similarly sized bubbles (ERG Aerospace Corporation, 2011). After solidification of the porous material, struts are formed between pores as the result of the intersection of adjacent bubbles. The porous materials of interest in the present work are isotropic in nature, such that neutrons, on the average, encounter the same total thickness of the strut material, per unit path length of travel, regardless of the directions the neutrons travel through the material.

* Corresponding author.
E-mail address: mar89@ksu.edu (M.A. Reichenberger).

http://dx.doi.org/10.1016/j.radphyschem.2016.08.021
0969-806X/

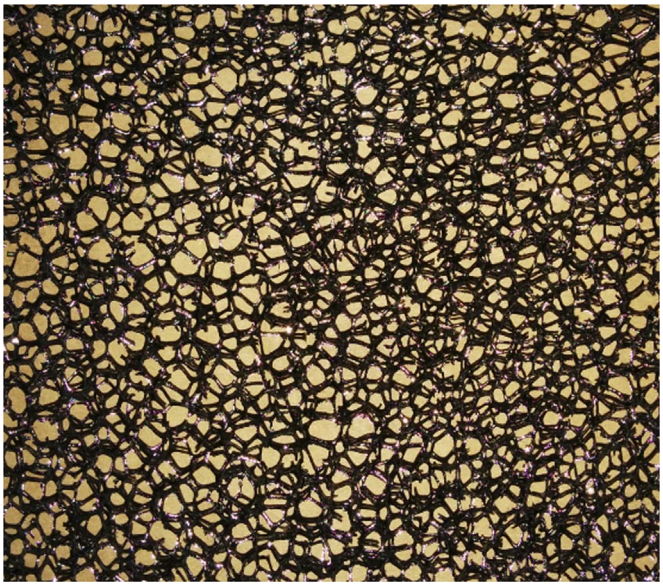

Fig. 1. Porous materials are composed of an interconnected network of solid struts which surround the gas-filled pores (ERG Aerospace Corporation, 2011).

Numerous porous materials are presently under investigation for possible use as neutron detectors; however, open-cell foam-based materials are of particular interest because of their extremely low cost and ease of fabrication (Nelson et al., 2012). Previous studies have investigated aerogels, ^{6}LiF-impregnated polyethylene foams, (Nelson et al., 2011) and boron-coated, reticulated vitreous-carbon (RVC) foams experimentally (Lavelle et al., 2013). Experimental work could be guided by the simulations capable of comparing various types of foam and geometric foam parameters. Although some attempts have been made to simulate such porous materials (Nelson et al., 2011), these earlier studies have suffered from one of two potentially limiting assumptions. First, ionization of the gas within the pores, inside the bulk of the material was neglected despite such ionization being critical to the intrinsic neutron detection efficiency (Lavelle et al., 2013). Second, although porous materials are composed of a heterogeneous system of pores and struts, past work approximated the porous materials by mass-conserving homogenization (Nelson et al., 2012). The results of this previous work have done well to advance the experimental progress towards a porous neutron detector; however, a more accurate simulation method is necessary.

In order to account for the ionization within the internal pores, particle transport must be modeled using an explicit representation of the complicated foam geometry. However, the random nature of heterogeneities comprising the interior of porous materials greatly complicates the development of a fully-defined geometric model for use in commonly used particle transport software packages. Specialized methods to simulate Monte Carlo ion transport can overcome some of the limitations of particle transport software packages. Two different methods were used in the present work to simulate porous materials for use as neutron detectors. First, a script was written in Python to generate an input file for use in the Monte Carlo Neutral Particle version 6 (MCNP6) software package. MCNP6 is a general-purpose Monte Carlo simulation code used for neutral particle, electron, and ion transport (Tsoulfanidis, 1995). A simple benchmark porous material problem was solved using MCNP6 and a novel Dynamic Path Generation (DPG) Monte Carlo method, developed and described here. The DPG method can accommodate more complex problems involving random heterogeneities. In lieu of adequate experimental data, a benchmark problem was solved with both methods to validate the DPG method.

2. Monte Carlo simulation methods

While previous studies have made progress in the simulation of porous media for neutron detection, most methods have required unrealistic assumptions about the material and, typically, neglect ionization occurring within the pores inside the bulk of the porous material (Lavelle et al., 2013). The amount of ionization which occurs within the pores inside the bulk of a porous material is one of the possible advantages of these materials but depends greatly on the geometry within the foam material, specifically the strut and pore dimensions. Simulations that can closely predict the response of a neutron reactive porous material to a thermal-neutron flux were developed here using MCNP6 simulations to serve as benchmarks for a new DPG method for treating random media.

Monte Carlo simulation is commonly used to solve complex particle transport problems (Dunn and Shultis, 2012). In the present case, the problem involves complex geometries and involves coupled neutron and ion transport calculations. The MCNP6 software package was the first choice when considering the simulation of porous materials for neutron detection. Both MCNP6 and custom Monte Carlo simulations have been used to predict the effectiveness of coated diode neutron detectors in the past (Shultis and McGregor, 2009). Although porous materials are composed of a heterogeneous system of pores and struts, past work has approximated porous materials by homogenization (Nelson et al., 2011; Lavelle et al., 2013). Homogenized simulation can adequately approximate the total neutron absorption in a porous medium, but cannot accurately estimate the ionization in the fill gas, which is the primary consideration of this work.

2.1. Dynamic path generation Monte Carlo simulation

One difficulty in simulating porous materials is the random nature of the interior heterogeneities. The isotropic distribution of pores of various sizes within the porous material makes the creation of a three-dimensional geometric model difficult and must first be characterized.

2.1.1. Geometric approximations and sampling distributions

The two types of foams that were simulated for the present work were characterized using a scanning electron microscope (SEM) to measure the strut thickness, pore diameter, and neutron-reactive coating thickness (where applicable) in numerous locations. After imaging LiF impregnated foam samples, the struts were approximated as right circular cylinders. In contrast, the RVC foam samples were observed to possess struts which were shaped approximately like equilateral triangular prisms. The thickness of the struts was measured from the center of each side of the strut as depicted in Fig. 2. The neutron-reactive coating thickness was also measured for struts as shown in Fig. 3. Both LiF impregnated foam and RVC foam had gas-filled pores that resembled circular openings, the diameter of which was measured from several locations, as illustrated in Fig. 4. The measurements to characterize the critical geometric parameters were repeated over numerous locations for foam samples with six different pore densities (5, 10, 20, 30, 45, and 80 pores per inch (PPI)). An average value and standard deviation were calculated from the SEM measurements, summarized in Table 1. A histogram of measured pore diameters for an 80 PPI foam sample is shown in Fig. 5. The values listed in Table 1 were based on a relatively small number of measurements (typically <50 measurements). The error associated with these measurements is noticeable and is captured in the standard

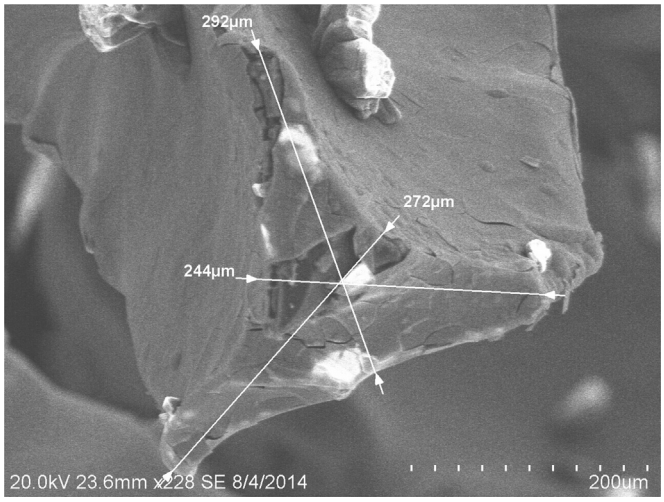

Fig. 2. Foam strut thicknesses were measured from several points on numerous foam samples using SEM measurements. An RVC foam sample is depicted here.

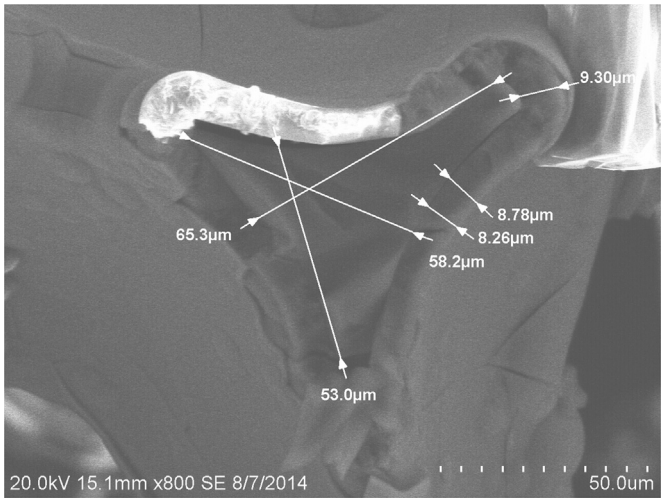

Fig. 3. Neutron-reactive coating thicknesses were obtained using SEM measurements.

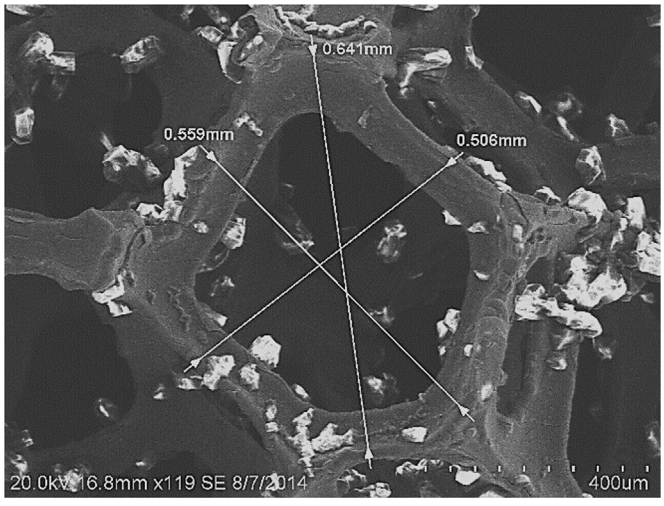

Fig. 4. Foam pore diameters were measured in several locations using SEM images and were approximated as spheres in the DPG simulation.

Table 1
Average values and standard deviations were calculated for pore diameter and strut thickness based on SEM measurements of foam samples.

Type of foam	Pore diameter (μm)	Strut thickness (μm)
LiF impregnated	500 ± 200	40 ± 10
5 PPI Coated RVC	4850 ± 810	418 ± 117
10 PPI Coated RVC	4000 ± 540	349 ± 83
20 PPI Coated RVC	3260 ± 460	285 ± 72
30 PPI Coated RVC	1940 ± 340	218 ± 56
45 PPI Coated RVC	1470 ± 150	120 ± 40
80 PPI Coated RVC	630 ± 120	50 ± 11

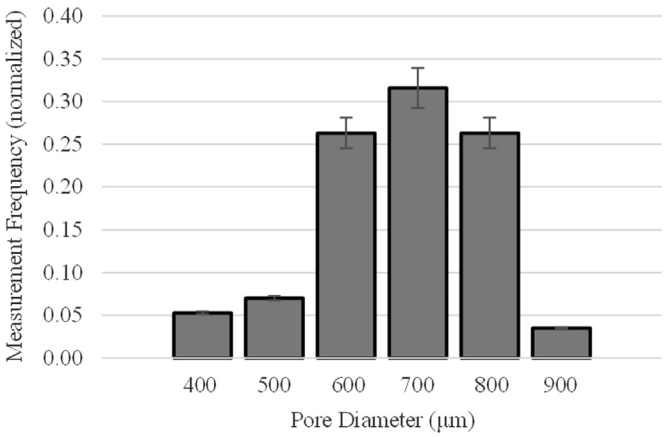

Fig. 5. The distribution of pore diameters for an 80 PPI foam sample can be approximated by a uniform distribution centered about the average value and extending one standard deviation in both directions.

deviation of the parameter measurements. The utilization of SEM imaging to measure the geometric parameters of the DPG method did introduce error into the simulation when compared to reality. However, error from the SEM analysis was uniform between both the MCNP6 and DPG simulation methods and should not compromise the validation process. Additional sample analysis should be used in the future to develop a more accurate probability distribution of feature sizes. A model for neutron and ion transport is described here which utilizes the values from Table 1 to simulate transport and reaction product ion energy deposition in porous materials.

2.1.2. *Dynamic path generation concept*

The DPG method reduces the complex, three-dimensional structure of porous materials to a simple, one-dimensional Monte Carlo model. This reduction is possible only because thermal neutrons and reaction product ions travel in straight line paths through the foam. A neutron travels in a straight line through pores and struts until it causes an absorption reaction; $^{10}B(n,\alpha)^{7}Li$ and for $^{10}B_4C$-coated foams, and $^{6}Li(n,t)^{4}He$ for ^{6}Li-impregnated foams (scattering interactions are negligible). Likewise, ions travel in straight lines through the pores and struts until their energy is dissipated through ionization and excitation of the ambient atoms. Large-angle scattering and straggling effects are neglected for ions. The DPG method shifts the perspective from that of an observer viewing the material, to that of a particle (neutron or ion) traveling through the material. Rather than using a static geometry, a dynamic path is generated for each particle history to emulate the random nature of the porous material structures in a defined space. This transformation is depicted in Fig. 6. The true path of a through numerous, randomly-oriented struts and pores (modeled as rectangles and circles), is shown in Fig. 6A. The path of Fig. 6A can then be modeled by an equivalent 1-D straight-line path by

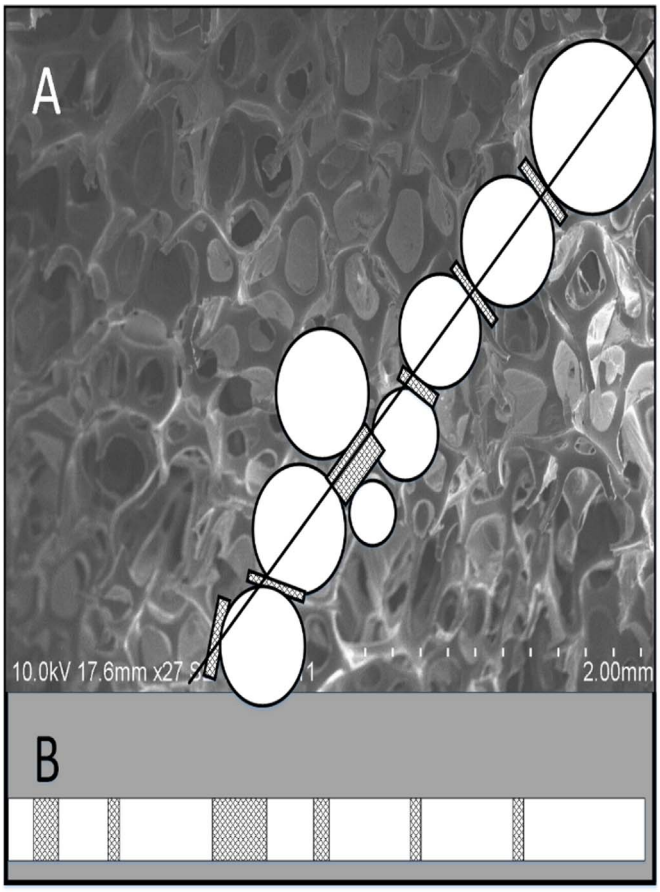

Fig. 6. Evolution of the particle (neutron or ion) path model used for dynamic path generation.

examining the chord length of the particle path through the individual struts and pores. This reduction to a 1-D trajectory is shown in Fig. 6B. The DPG method significantly reduces computation time by generating cells and path lengths dynamically, only for cells through which a particle passes. Finally, in order to model the three-dimensional structure of the porous material properly, the structure was characterized and approximated by simple shapes, such as the rectangles and circles used here, which are then used in the DPG simulation. The details of the DPG method for both neutrons and reaction product ions are discussed in more detail below.

2.1.3. *Neutron transport*

The principal purpose of the present work was to predict the scatterless intrinsic thermal-neutron detection efficiency of porous materials in an optimal environment. Appropriately, the neutron source in the DPG Monte Carlo simulation described here emitted only thermal neutrons (0.025 eV) (Duderstadt and Hamilton, 1976). Additionally, neutron scattering was neglected, and only the absorption cross sections for neutron-reactive materials were considered (σ_{6Li}=940 barns, σ_{10B}=3842 barns) (National Nuclear Data Center (NNDC), 2014). The probability of neutron interaction in the ionizing gas and non-lithium/boron components of the foam was assumed to be zero. The source effectively simulated uniform irradiation of a sample by using a new particle path model for each neutron history (emulating neutrons emitted toward different parts of a large sample). Each neutron history was initialized normal to the surface of the sample.

When a neutron encountered a strut, a strut thickness t and strut length L were determined by sampling from a uniform distribution which varied $\pm 1\sigma$ about the mean thickness of the strut with the mean thickness and σ listed in Table 1. The uniform distribution was used based on qualitative assessment of the SEM measurements, as illustrated in Fig. 5. The thickness of strut material through which the neutron travels depended on the orientation of the strut relative to the direction of the neutron as well as the point of intersection of the neutron and strut. The path length of the neutron through the strut was found by first uniformly sampling an intersection distance I (the point along the length of the strut where the neutron path intersects the strut, $I \in$ [0, ½] strut length) and transmission angle Ω (the angle of the strut relative to the incident neutron path, $\Omega \in [0, 2\pi]$ steradians), as illustrated in Fig. 7. Then, the path length of strut material along the trajectory of the neutron was calculated. Next, an interaction distance d was sampled using the Inverse CDF method (Dunn and Shultis, 2012) for an exponential decay, namely as $d = -ln(\rho)/\Sigma$ where Σ is the macroscopic neutron absorption cross section for the strut, and ρ is a uniformly-sampled pseudo-random number between 0 and 1. Pseudo-random numbers for the DPG Monte Carlo simulation were all obtained using a standard Park and Miller minimal standard pseudorandom number generator (Dunn and Shultis, 2012).

If $d > t$ then no neutron interaction was simulated in the strut material and a pore was created. The neutron was then transported through the pore. Before a path length for the pore was determined, the pore diameter was sampled (similarly to strut thickness), and transmission angle through the pore was determined ($\Omega \in [0, 2\pi]$ steradians). Once the pore diameter and transmission angle were sampled, the neutron path length through the pore was determined. Although no neutron interactions were simulated for the gas within the pore, the distance traversed by the neutron through pores must be recorded to determine when the neutron had exceeded the dimensions of the sample. If the neutron traveled farther than the dimensions of the sample material, the history ended by increasing the 'escaped

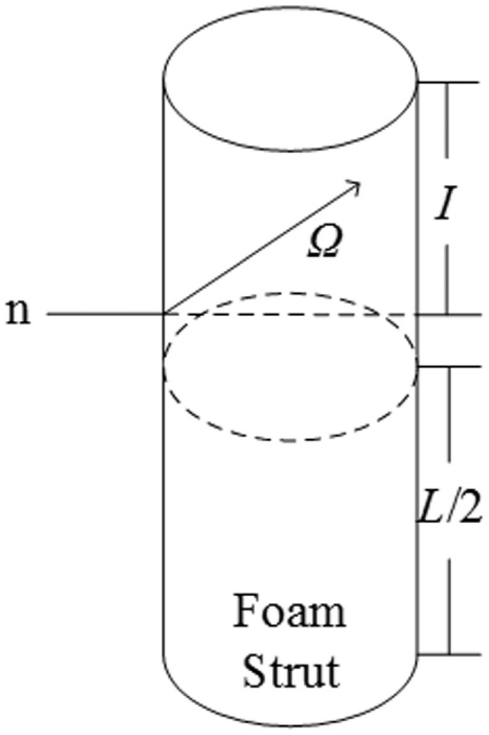

Fig. 7. The intersection distance I, and transmission angle Ω, are selected uniformly to simulate the various angles of struts that an incident neutron may encounter in a porous material.

neutron' tally by one.

However, if $d < t$ the neutron interaction was simulated at distance d into the strut along the transmission angle direction Ω. The 'captured neutron' tally was incremented by one, and the location of the neutron interaction was then used to begin the simulation of the reaction product ions through the porous material.

2.1.4. Reaction product ion transport

When a neutron interaction was simulated in the strut material, the penetration distance x and offset length y were pre-determined by the interaction location. The location of the neutron interaction was then translated to the strut coordinate system by the location vector $\underline{r}$, as illustrated in Fig. 8(A) and (B). After randomly selecting an ejection angle for one reaction product ion (uniformly within 4π steradians), the directional cosines ($\alpha = \hat{\mathbf{i}} \cdot \underline{\mathbf{r}}$, $\beta = \hat{\mathbf{j}} \cdot \underline{\mathbf{r}}$, $\gamma = \hat{\mathbf{k}} \cdot \underline{\mathbf{r}}$) were calculated as illustrated in Fig. 8(C) and (D). Then, the remaining reaction product ion was generated with an ejection angle opposite of the first ion. The path length to the edge of the strut $\underline{p}$ was then calculated for each reaction product ion as illustrated in Fig. 8(E). The cases in which one or both reaction products exit through the top or bottom of a strut were also considered, but are not depicted. After the first path length of the reaction products were determined, the energy of the reaction products exiting the strut was determined using the residual energy method (Shultis and McGregor, 2007). A pore was then generated using the same sampling method as was used for neutron transport. Subsequent transport of the charged particles continued through pores and struts until the energy of the reaction products reached 0 eV. Often, the neutron interaction distance and emission angles were such that one or both reaction products did not escape the strut material, a common problem in neutron detection (Shultis and McGregor, 2009). However, any reaction product energy lost during transport through a pore was tabulated as recoverable ionization for the history. At the conclusion of the history, the total energy deposited via ionization in all pores was recorded.

2.1.5. Energy deposition and the pulse height spectrum

Ion energy deposited within the porous material was recorded only if the energy was deposited within a pore. The ideal case for porous material-based neutron detectors assumes that all ionization within the gas pores was collectable by an applied bias across the sample. The assumption that all ionization is collectable yields the maximum possible signal for the simulated material. Real-world electron-ion propagation through porous materials will likely not be complete, thus the efficiency of prototype devices is expected to be less than ideal. However, signal degradation by incomplete charge collection was not considered in this study. By maintaining a list of the energy deposited in the pores for each neutron history, a histogram of these energies can be created and represents the ideal pulse height spectrum (PHS) expected from the sample. A lower-level discriminator (LLD) setting was used during the PHS development to exclude histories with low ion-energy deposition (much like an LLD would be used in an experiment to exclude low-amplitude pulses). Such a PHS is illustrated in Fig. 9. The maximum simulated thermal-neutron detection efficiency, ε_{th}, of a sample was then calculated as the number of counts recorded above the LLD setting divided by the number of neutron histories.

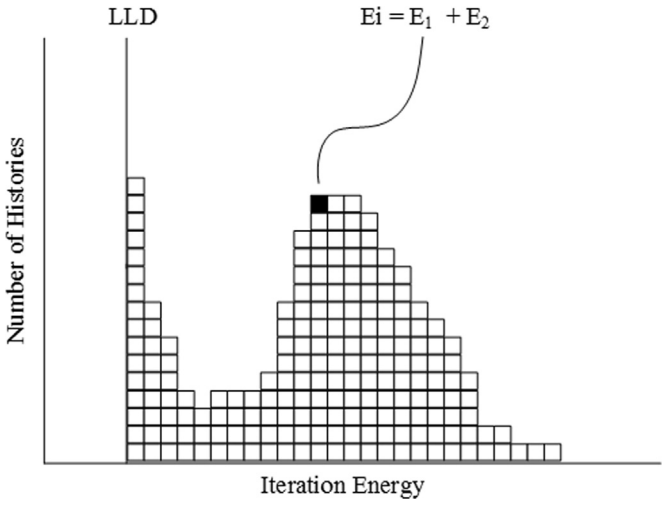

Fig. 9. Energy bins were used to build a PHS for the DPG Monte Carlo simulation.

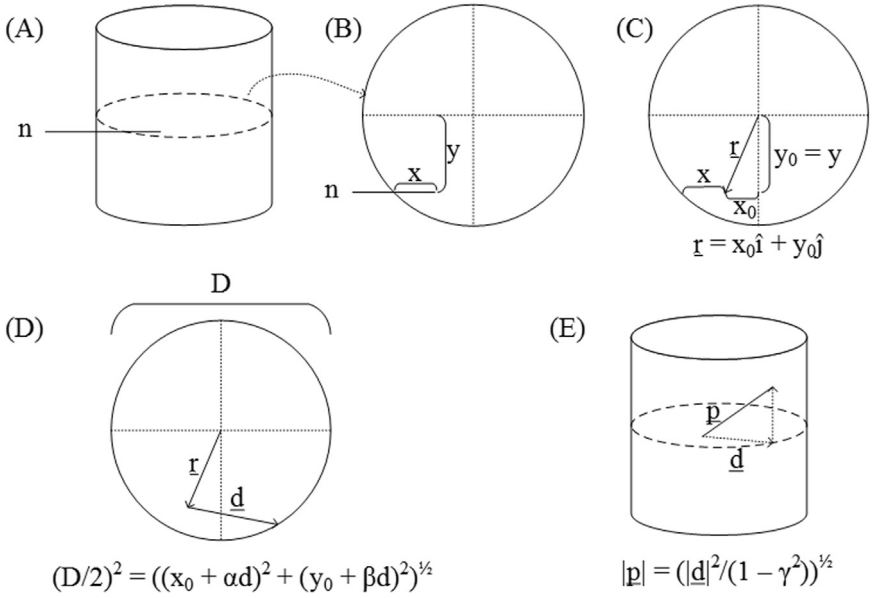

Fig. 8. The path-length of the reaction products through the strut in which they are born is calculated using vector math. The x and y positions represent the location of the neutron interaction (A and B). The $\underline{\mathbf{r}}$ vector represents the neutron interaction location with respect to the origin of the strut (C). The $\underline{\mathbf{d}}$ vector represents the projection of the path of the reaction product in the xy plane (D). The total path-length is represented by the $\underline{\mathbf{p}}$ vector (E).

2.1.6. Necessity of DPG validation

During development of the DPG method, it became evident that some validation of the method was required to ensure that the results of the simulation were correct. An early attempt was made to match DPG simulation results to preliminary experimental work, but inconsistency between the experimental setup and simulation design introduced concern about the results (Reichenberger et al., 2014). As an alternative verification method, an MCNP6 simulation method for porous materials was developed. The validation of the DPG method using a well-accepted particle-transport simulation environment can support the use of the DPG method in more complicated scenarios in which MCNP6 is not capable of modeling the geometry, as described below.

2.2. MCNP6 simulation

From the macroscopic point of view, the simulation of porous materials is not a complex problem. Unlike many other MCNP simulations, the present work involves relatively few variables, which include a foam volume (consisting of strut material with gas pores) surrounded by a gaseous medium. The inclusion of tabulated neutron interaction cross-sections and charged particle models makes MCNP6 simpler to implement than custom simulations. The clever selection of tally volumes with the ability to tally various events makes the development of a pulse height spectrum (PHS) and calculation of detector efficiency simple as well. Finally, visualization using the MCNPX Visual Editor tool and relatively fast execution time (for the present work) greatly aid in the troubleshooting process of simulation development (Pelowitz, 2011). For these reasons MCNP6 simulation was chosen as a method to simulate porous materials for neutron detection. In fact, MCNP has been applied to similar problems, also with stochastic geometries, such as pebble-bed nuclear reactor cores (Kim et al., 2011; Hosseini, 2012). The most difficult step in the development of an MCNP6 simulation input for porous materials is the generation of the fully-defined foam geometry.

2.2.1. MCNP6 input generation

To model heterogeneous structures, a repeating lattice is commonly used. However, the use of a lattice structure eliminates the random nature of the porous material. An accurate geometric model of a porous material should include discrete, heterogeneous regions representing struts and pores, randomly placed within the sample volume. Generating such an input geometry for MCNP6 manually would require significant effort. However a script can automate the generation of a random, porous interior of a foam sample for an MCNP6 simulation. Such a script was written in Python to select pore locations and dimensions, and create a useable MCNP6 input file. The script was used to create MCNP6 input files for either impregnated polyethylene foams or coated RVC foams. A characteristic section of a 20 PPI lithiated foam sample, generated using the MCNPX Visual Editor software package, (Pelowitz, 2011) is depicted in Fig. 10.

2.2.2. Limitations of MCNP6

The primary limitation of MCNP6 for the present work is the maximum character length allowed for cell definition cards, namely 9999 characters (Pelowitz, 2013). To define the pores within a porous material requires the specification of all of the surfaces comprising the pores. In addition, the definition of the struts requires reference to the cell containing the pores. To simulate coated materials, a third cell definition must be made for the material layer on the struts that references the 'struts' and 'pores' cells. Each new feature (pore, strut, layer, etc.) further reduces the effective number of pores that can be simulated. In the case of layered foams, the maximum length of the cell specification card severely limits the number of pores that can be modeled. For this reason, only small samples with relatively large pores may be simulated with MCNP6 without exceeding the limitation of cell specification character length.

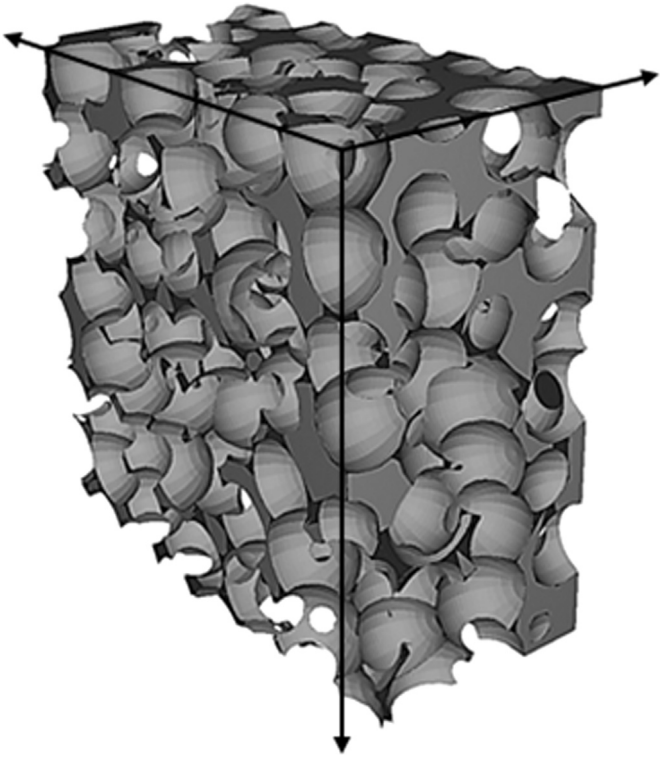

Fig. 10. The MCNPX Visual Editor software package was used to visualize a portion of the 20 PPI foam simulated for the validation of the DPG method.

2.3. DPG validation test cases using MCNP6

For the validation test case, a 1-cm thick, 2-cm tall, 2-cm wide, 20 PPI, LiF impregnated (lithiated) foam sample was simulated by both MCNP6 and by the DPG method. Lithiated foam was selected because coated devices significantly increase the length of the foam cell definition in the MCNP6 input file, further limiting the size of sample that could be modeled. The maximum theoretical impregnation level for the foams which were analyzed in the present work was 27.5% ^{6}LiF by weight. A conservative impregnation level of 20% was used as a realistic estimate, an enrichment that allows some neutrons to escape the sample without interacting. The 1-cm × 2-cm × 2-cm foam sample provided ample volume to create several layers of pores within the sample, while also extending far enough in each direction to limit the number of reaction products that escape the bulk of the foam. The sample was surrounded by a void to prevent escaped reaction products from depositing additional energy outside of the foam. Reaction product ions which escaped the sample were neglected because only the ionization that occurs within the pores of the bulk of the foam is of interest for the DPG method. Thus, only energy deposited by reaction product ions within the pores of the foam was tallied.

2.3.1. DPG test case approximations

The DPG method relies on several assumptions not used in MCNP6. First, neutron scattering is neglected. The neutron-scatter cross-section for thermal neutrons in a lithiated material is significantly smaller than the neutron-absorption cross section; however, some scattering is likely to occur in a test environment.

Second, a point source of thermal neutrons was used which emulates a uniform irradiation by selecting a new path for each neutron history. The use of a completely new path for each history may artificially suppress the effects of streaming through the thin test sample which was used because of the limitations of MCNP6. Neutron interactions in all materials except the lithiated strut are neglected.

2.3.2. MCNP6 test case approximations

The primary approximation made in the MCNP6 simulation is in the geometry of the sample. The MCNP6 simulation utilized a disk source of mono-energetic, mono-directional thermal neutrons with a 0.5 cm radius placed 0.1 cm from the surface of the foam sample. Uniform sampling of the disk area was used in order to create various neutron paths during the simulation. However, correlations to the particular sample geometry were still a concern. Neutron streaming paths are depicted in Fig. 10 as white regions, through which a neutron streams through the sample without encountering any strut material. To reduce the effect of static geometry, the MCNP6 validation was repeated 10 times, using foam samples which were independently generated and an average tally value was used (simulation error was propagated using a root-mean-square average error for the result). For all cases (MCNP6 and DPG) 10^6 particle histories were used.

2.3.3. Test case comparisons

The test case described above was simulated using both MCNP6 and the DPG method. In both cases, it was determined that the simulated intrinsic thermal-neutron detection efficiency of the samples were $<0.5\%$. Since ten different MCNP6 simulations were executed (all with the same parameters, but with randomly selected pore locations), an average value was obtained. The average simulated intrinsic thermal-neutron detection efficiency of a 20 PPI, 20% ^{6}LiF impregnated polyethylene foam obtained with MCNP6 was $0.470 \pm 0.034\%$. Similarly, the DPG method yielded a simulated intrinsic thermal-neutron detection efficiency of $0.471 \pm 0.007\%$. The PHS from the MCNP6 simulation that yielded an efficiency closest to the average value ($0.472 \pm 0.007\%$) is shown in Fig. 11. The PHS shows an exponential attenuation in the likelihood of an interaction with respect to energy bin. The low detection efficiency of the simulated foam and the shape of the PHS can both be attributed to the small pore size compared to the reaction product ion ranges in argon (at 1 atm), and the dispersion of neutron reactive material throughout the thick struts. The average pore diameter for the 20 PPI foam sample was 500 μm. Comparatively, the average ranges of the lithium reaction products (alpha particle and triton) in 1 atm argon are 12 mm and 70 mm, respectively (Ziegler and Biersack, 2013). Bragg ionization, which characterizes the energy deposition of such charged particles, dictates highly localized ionization near the end of the particle range (Tsoulfanidis, 1995). Very little energy from each reaction product is deposited in the ionizing gas because the argon-filled pores constitute only a small portion of the total reaction product path length. The most probable case for an interaction to deposit sufficient energy in the ionizing gas to exceed the LLD of the simulation occurs when a reaction product is born sufficiently deep within the foam strut to lose a majority of its energy before entering the gas-filled pore. The particle then terminates within the pore, depositing what little energy it still possessed. The effects of the small pore size can be resolved by increasing the gas fill pressure (to increase specific ionization within the gas), increasing pore size, or by selecting a neutron-sensitive material which emits less penetrating reaction products (e.g., ^{10}B).

As an additional comparison, a 20 PPI RVC foam sample with 2.8 atm argon pressure and an LLD $=75$ keV was simulated with MCNP6. Because of the limitation of MCNP6 discussed above, only a 2-cm thick sample was simulated with a 1.3 μm $^{10}B_4C$ coating. This MCNP6 simulation yielded an intrinsic thermal-neutron detection efficiency of $32.15 \pm 2.80\%$ (averaged over ten independent simulations). The MCNP6 simulation was found to be very sensitive to variations in pore location, with efficiency results ranging from $28.1 \pm 0.05\%$, to $36.9 \pm 0.05\%$. These variations resulted in the large standard deviation for the MCNP6 simulation results which were averaged over ten independent simulations with the same parameters so that different pore locations were used for each simulation. The PHS for the MCNP6 simulation resulting in an intrinsic thermal-neutron detection efficiency of $31.67 \pm 0.05\%$ (near the average value of $\sim$31%) is shown in Fig. 12. The DPG method was also used to simulate a 2.0 cm sample of $^{10}B_4C$-coated RVC foam, yielding a simulated intrinsic thermal-neutron detection efficiency of $34.59 \pm 0.06\%$, and with the PHS depicted in Fig. 13. Spectral features from the 94% branching ratio of the (^{10}B+n) reaction are clearly visible in both the MCNP6 and DPG simulation results. In contrast to the MCNP6 simulation, however, the DPG simulation did not include contributions from the 6% branching ratio.

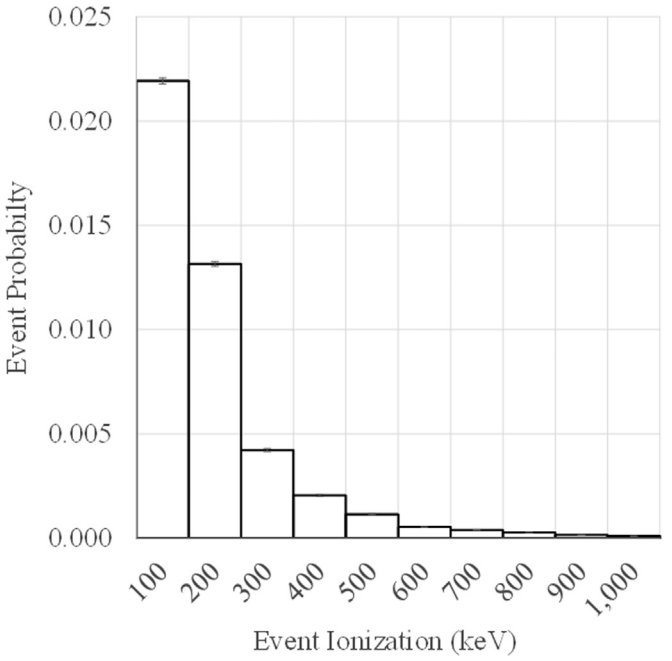

Fig. 11. The simulated PHS for 20 PPI, 20% 6LiF-impregnated foam shows a very low likelihood of a neutron interaction depositing sufficient energy to exceed the 300 keV LLD used in the simulation.

3. $^{10}B_4C$-coated RVC foam optimization using DPG

The optimization of a more complex problem was possible after the preliminary validation of the DPG Monte Carlo method to simulate foam materials. Lithiated foams are not very attractive as neutron detectors because of the long range of the high-energy reaction products and the small pore sizes available from the manufacturer. Consequently, the focus shifted toward the optimization of enriched boron-carbide-coated RVC foams. As previously described, the lower energy reaction products from the ^{10}B-based coating are more favorable for the small pores of ionizing gas present in the porous material. The thermal neutron-absorption cross section for ^{10}B is much larger than for ^{6}Li so that less neutron-sensitive material must be used. Boron-carbide (B_4C) coatings are used because of the superior durability of B_4C compared to pure boron (Lavelle et al., 2013).

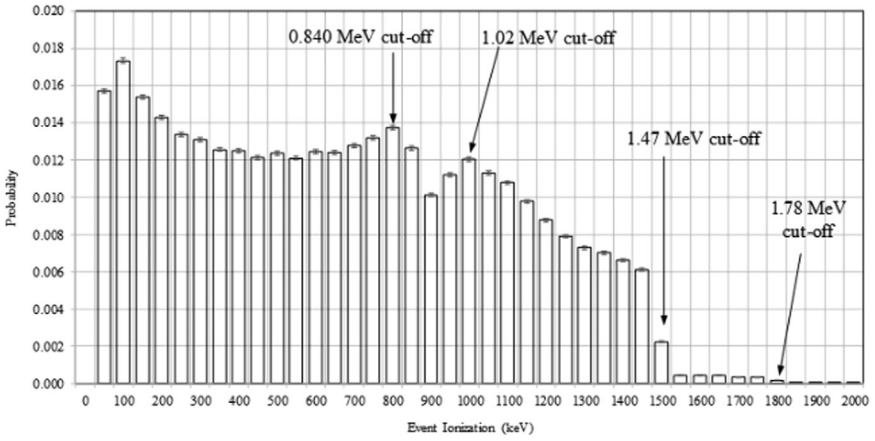

Fig. 12. Using MCNP6, the 20 PPI RVC foam with a 1.3 μm $^{10}B_4C$ coating yields a PHS with sharp cut-offs for all four $^{10}B(n,\alpha)^7Li$ reaction products. The additional energies in the 6% branch also contribute to the PHS.

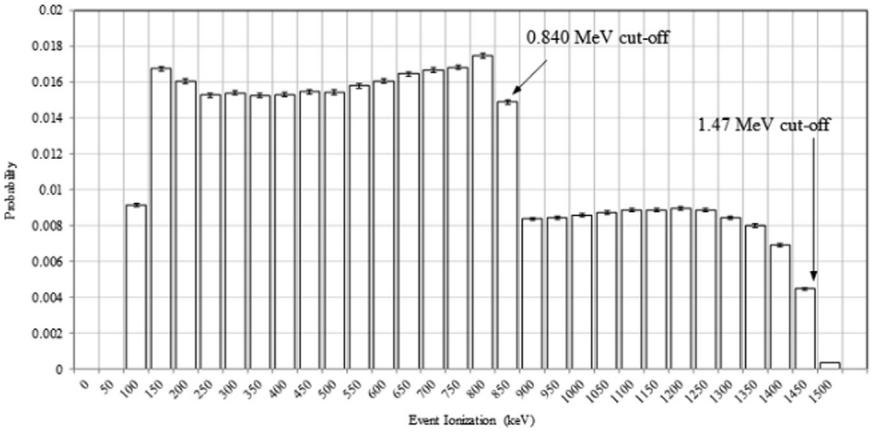

Fig. 13. Using the DPG method, the 20 PPI RVC foam with a 1.3 μm $^{10}B_4C$ coating yields a PHS with sharp cut-offs for two $^{10}B(n,\alpha)^7Li$ reaction product.

Foam-based neutron detectors can utilize the ionization deposited within the bulk of the foam material, as well as the energy deposited by escaping reaction products. Reaction product ions born within the interior of the foam sample rarely escape to the surrounding gas, especially as porosity increases. Thus, extraction of ionization in the pore gas is a great advantage for high-porosity foams. Pore density has three distinct effects on the simulated intrinsic thermal-neutron detection efficiency of a foam-based neutron detector. First, the smaller pores inherently result in a larger amount of neutron-reactive material present in the sample because each strut is conformally coated. Second, smaller pores present shorter ionization paths for the reaction product ions in the pore gas. Finally, reduced pore size increases neutron attenuation by reducing (or eliminating) neutron streaming paths (Lavelle et al., 2013). Previous studies have examined the effectiveness of B_4C-coated RVC foam utilizing only reaction product ionization exterior to the foam and focused on the use of thin (<2 cm), low-porosity samples in order to allow reaction product ions to stream out of the bulk foam into the exterior gas (Lavelle et al., 2013). The optimization of the thickness of the neutron-reactive material from these previous studies suggested an optimal $^{10}B_4C$ coating thickness >3 μm for samples ranging in porosity from 5 PPI to 45 PPI (Lavelle et al., 2013). By utilizing the interior ionization, greater simulated intrinsic thermal-neutron detection efficiency is possible, but the optimal B_4C coating thickness will be different from previous studies.

Optimal $^{10}B_4C$ coating thickness for RVC foams were found using the DPG method. Simulated samples all had a total cross-sectional thickness of 4.1275 cm. Foam porosities of 5, 10, 20, 30, 45, and 80 PPI were studied, using the SEM-measured parameters shown in Table 1.

3.1. Optimized $^{10}B_4C$ coated RVC foam results

The $^{10}B_4C$ coating optimization results for the previously described samples are summarized in Table 2. The results of the $^{10}B_4C$ coating thickness optimization show that much thinner neutron-reactive coatings are required for RVC foam-based neutron detectors than was suggested by previous studies (Lavelle et al., 2013). The LLD setting used in the simulation also has a drastic impact on the simulated intrinsic thermal-neutron detection efficiency of the sample. Additionally, increasing the pressure of the fill gas in the simulation increased simulated intrinsic thermal-neutron detection efficiency. Shown in Figs. 14–17, are optimization curves for the coated RVC foam samples with an LLD setting of 75 keV, 150 keV, and 300 keV, respectively, for a 1 atm argon pressure. The highest simulated intrinsic thermal-neutron detection efficiency was determined for an 80 PPI sample with an elevated argon gas pressure of 2.8 atm and an LLD $=75$ keV, as shown in Fig. 17. Increasing the pressure in the simulation increased the specific ionization in the gas pores, while decreasing the LLD allowed for more interactions to be counted. The optimal coating thickness varied based on the operating pressure and LLD setting. Hence, the fill gas pressure and LLD should both be considered when designing an optimized device for testing. The total cross-sectional sample thickness also affected the optimal coating thickness.

Table 2
Optimal $^{10}B_4C$ coating thicknesses and respective simulated intrinsic thermal-neutron detection efficiency simulated using the DPG method for a 4.1275 cm thick, coated RVC foam sample of various pore densities.

	75 keV LLD, 2.8 atm		75 keV LLD, 1.0 atm		150 keV LLD, 1.0 atm		300 keV LLD, 1.0 atm	
Porosity	***Optimal thickness***	***Simulated detection efficiency***	***Optimal thickness***	***Simulated detection efficiency***	***Optimal thickness***	***Simulated detection efficiency***	***Optimal thickness***	***Simulated detection efficiency***
5 PPI	1.1 μm	39.4 ± 0.20%	1.0 μm	39.2 ± 0.20%	0.9 μm	36.8 ± 0.19%	1.1 μm	32.4 ± 0.18%
10 PPI	0.9 μm	42.1 ± 0.21%	0.8 μm	42.1 ± 0.21%	0.9 μm	39.1 ± 0.20%	0.8 μm	34.1 ± 0.18%
20 PPI	0.8 μm	44.4 ± 0.21%	0.8 μm	44.1 ± 0.21%	0.7 μm	41.5 ± 0.20%	0.6 μm	36.2 ± 0.19%
30 PPI	0.5 μm	49.3 ± 0.22%	0.5 μm	49.1 ± 0.22%	0.5 μm	45.2 ± 0.21%	0.5 μm	37.8 ± 0.19%
45 PPI	0.3 μm	54.3 ± 0.23%	0.4 μm	53.2 ± 0.23%	0.3 μm	49.0 ± 0.22%	0.3 μm	39.5 ± 0.20%
80 PPI	0.2 μm	62.8 ± 0.25%	0.2 μm	58.6 ± 0.24%	0.2 μm	49.2 ± 0.22%	0.2 μm	34.6 ± 0.19%

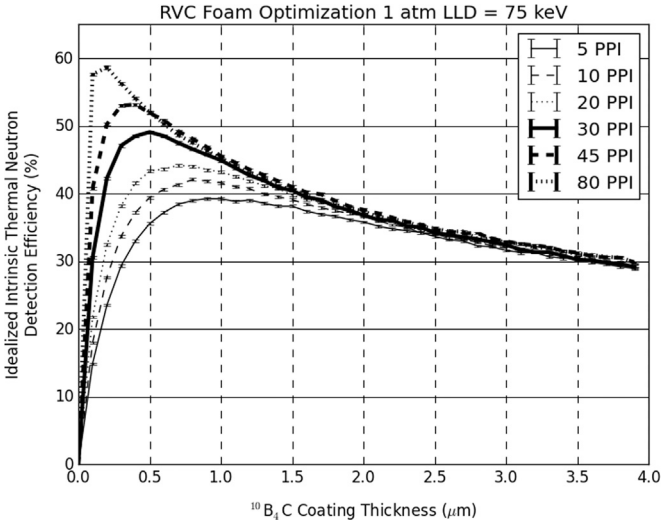

Fig. 14. A 45 PPI $^{10}B_4C$-coated RVC foam sample with a total cross-sectional thickness of 4.1275 cm yields a simulated thermal-neutron detection efficiency of 53.2 ± 0.23% for an LLD = 75 keV with a 0.4 μm thick coating.

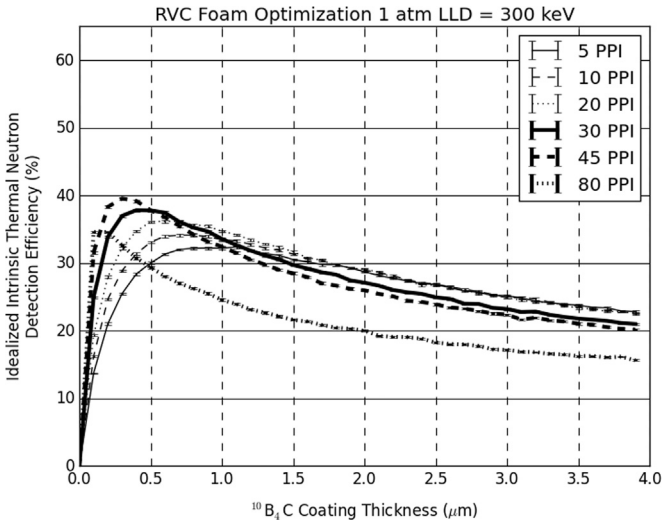

Fig. 16. An LLD = 300 keV further reduces the simulated thermal-neutron detection efficiency for each foam sample. Low porosity samples (5, 10, and 20 PPI) are affected less than higher porosity samples (30, 45, and 80 PPI).

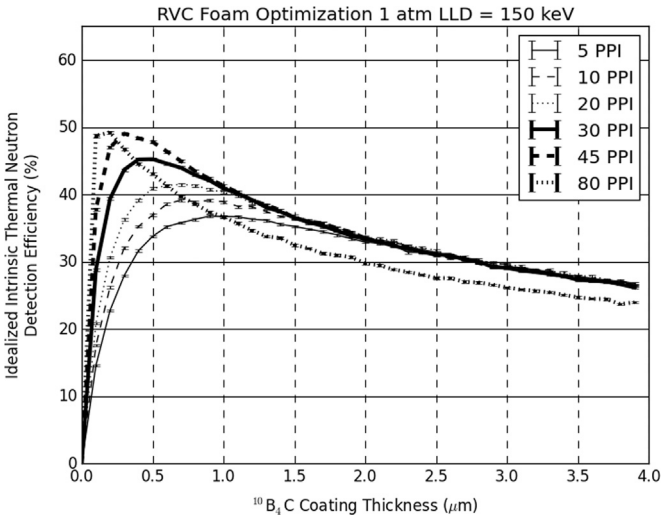

Fig. 15. Increasing the LLD in the simulation suppresses the simulated thermal-neutron detection efficiency for all porosities of coated RVC foams. For an LLD = 150 keV, a 20 PPI foam coated with 0.7 μm of $^{10}B_4C$ yields a simulated thermal-neutron detection efficiency of 41.5 ± 0.20%.

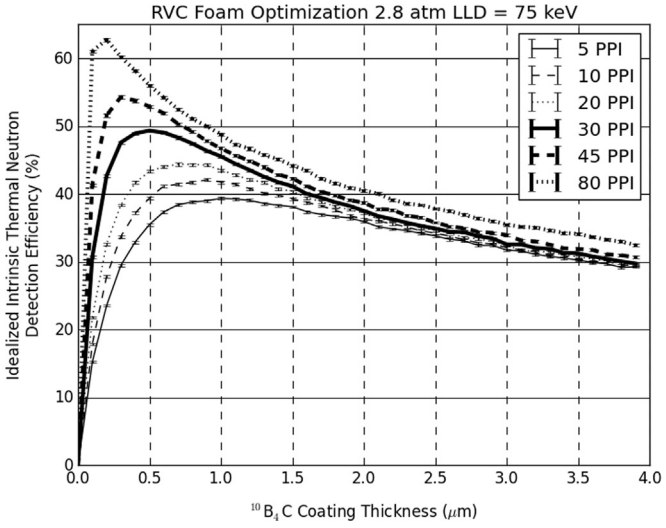

Fig. 17. Increasing the ionizing gas pressure increases the simulated intrinsic thermal-neutron detection efficiency of the foam samples. Using an argon pressure of 2.8 atm, 80 PPI RVC foam with a 0.2 μm thick $^{10}B_4C$ coating yields a simulated thermal-neutron detection efficiency of 62.8 ± 0.25% for an LLD = 75 keV.

4. Conclusions

The DPG Monte Carlo method has been used to determine the optimal coating thicknesses for $^{10}B_4C$-coated RVC foams with porosities of 5, 10, 20, 30, 45, and 80 PPI. In order to validate the DPG method, a Python script was written to generate MCNP6 input files for small impregnated- and coated-foam samples. The MCPN6 simulation and DPG simulation yield results with a few notable differences for the test cases designed for validation of the DPG method as illustrated in Fig. 11, Fig. 12, and Fig. 13. The PHS calculated for the 20 PPI RVC foam using MCNP6 and the DPG method depict several differences, each an embodiment of one of the assumptions made for the DPG method. Most prominently, the MCNP6 results include the 6% branch of the ^{10}B reaction creating a rise in the PHS at 1.02 MeV, and a tail extending to 1.78 MeV, features which are not present in the DPG method PHS. The MCNP6 PHS also shows a higher proportion of low-energy pulses, contributions from ions born within the bulk of the strut material. Low-energy reaction products are more likely in the MCNP6 simulation due to the thicker struts, depicted in Fig. 10. The preference towards lower-energy pulses for the MCNP6 results also reduces the simulated intrinsic thermal-neutron detection efficiency.

4.1. Optimal device parameters

As shown in Table 2, the optimal $^{10}B_4C$ coating thickness depends heavily on the foam porosity, LLD setting, and pressure of the fill-gas. The highest simulated intrinsic thermal-neutron detection efficiency ($62.8 \pm 0.25\%$) simulated in the present work utilized 80 PPI RVC foam with a 0.2 μm thick coating of $^{10}B_4C$, an LLD $=75$ keV, and argon pressure of 2.8 atm. If an LLD setting of 300 keV is required (due to high gamma ray background activity or electronic noise), and atmospheric pressure is used, the lower-porosity foam (5–45 PPI) performance exceed that of the 80 PPI sample drastically. Further increasing the argon pressure could indeed increase the simulated intrinsic thermal-neutron detection efficiency of coated RVC foam-based thermal neutron detectors; however other factors must also be considered, such as charge collection, to continue the development of these devices.

4.2. Simulation improvements

The DPG method has been used to simulate neutron and charged reaction product transport through porous materials. However, further improvements to the simulation will improve the application of the DPG method. The variation between the DPG method and MCNP6 simulations of the optimized 20 PPI $^{10}B_4C$ cause concern that both simulation methods could be improved. As previously discussed, the MCNP6 simulation is severely limited by the constraints of the software package (namely the 9999 character limit for cell definitions). One way to avoid this limitation is to create an MCNP6 input file which has different strut and pore cell definitions for various regions within the sample. Using this advanced input file generation scheme would limit the number of characters in each individual cell definition while expanding the overall size of the foam sample that could be simulated. Increasing the sample size would also reduce variation between MCNP6 simulations. Several improvements can also be made to the DPG Monte Carlo method used for porous materials, as described below.

Currently, only ionization within the pores inside the bulk of the foam material is considered. Some research has considered the application of multiple thin (<1 cm) layers of foam material (Nelson et al., 2012), in which the ionization outside of the bulk material is significant. The consideration of the 6% branch of the ($^{10}B_4C+n$) reaction would also increase the fidelity of the DPG Monte Carlo simulation.

Most importantly, a re-assessment of the parameter distributions (e.g., strut thickness and pore diameter) could greatly improve the accuracy of the DPG Monte Carlo simulation. With more precise measurements from sample foams, and the use of more appropriate probability distribution functions, the parameters would yield a more accurate representation of the foam geometry. Of particular interest is the curvature of the struts within the foam. In the current simulation, the neutron-reactive coatings are considered planar with respect to the range of the reaction products (<5 μm); but, in reality, a curvature exists which may extend or shorten the path length of the reaction products through the neutron-reactive coating. This curvature affects the solid-angle for which reaction products can escape the foam strut, possibly changing the simulated intrinsic thermal-neutron detection efficiency of such devices. The impact of strut curvature is unknown at this time; however, a correlation between pore-diameter and strut curvature is expected to exist. Improvement of the DPG path model will lead to a more accurate geometric model, and greater simulation accuracy. Currently, there is no method by which the true accuracy of the DPG simulation can be measured. A comparison to MCNP6 was made in order to validate the process; however, even the MCNP6 simulation is not a prefect representation of the foam geometry. Experimental verification of the simulated intrinsic thermal-neutron detection efficiency of foam-based neutron detectors is needed.

References

Duderstadt, J.J., Hamilton, L.J., 1976. Nuclear Reactor Analysis. Wiley & Sons, Inc, New York.

Dunn, W.L., Shultis, J.K., 2012. Exploring Monte Carlo Methods. Academic Press, Amsterdam, Netherlands.

ERG Aerospace Corporation, 2011. "The Basics of Duocel Foam," ERG Aerospace Corporation. (Online). Available: ⟨http://www.ergaerospace.com/Descriptors.htm⟩. (accessed 22.01.15).

Hosseini, S.A., 2012. A New Random Distribution Method to Simulate PBM Type Reactors with MCNP. Ann. Nucl. Energy no. 50, 215–219.

Kim, H., Kim, S.H., Kim, J.K., 2011. A new strategy to simulate a random geometry in a pebble-bed core with the Monte Carlo code MCNP. Ann. Nucl. Energy 38, 1877–1883.

Lavelle, C.M., Deacon, R.M., Hussey, D.S., Coplan, M., Clark, C.W., 2013. Characterization of boron coated vitreous carbon foam for neutron detection. Nucl. Instrum. Methods Phys. Res. A 729, 346–355.

National Nuclear Data Center (NNDC), 2014. Evaluated Nuclear Data File (ENDF). Brookhaven National Laboratory, New York.

Nelson, K.A., Neihart, J.L., Riedel, T.A., Schmidt, A.J., McGregor, D.S., 2012. A novel method for detecting neutrons using low density high porosity aerogel and saturated foam. Nucl. Instrum. Methods Phys. Res. A 686, 100–105.

Nelson, K.A., Bellinger, S.L., Montag, B.W., Neihart, J.L., Riedel, T.A., Schmidt, A.J., McGregor, D.S., 2011. Investigation of aerogel, saturated foam, and foil for thermal neutron detection. In: Proceedings of the Conf. Rec. IEEE Nuclear Science Symposium. Valencia, Spain, Oct. 23–29, 2011.

Pelowitz, D.B. (Ed.), 2011. MCNPX User's Manual Version 2.7.0. Los Alamos National Laboratories, New Mexico.

Pelowitz, D.B., 2013. MCNP6 User's Manual, Los Alamos National Security, LLC.

Reichenberger, M.A., Fronk, R.G., Shultis, J.K., Stevenson, S.R., Edwards, N.S., Nelson, K.A., McGregor, D.S., 2014. Monte Carlo simulation of energy deposition by neutron reaction products in lithiated foam using dynamic path generation. In: Proceedings of the Conf. Rec. IEEE Nuclear Science Symposium, Seattle. Nov. 8–15, 2014.

Shultis, J.K., McGregor, D.S., 2007. Calculation of Ion Energy-Deposition Spectra in Silicon, Lithium-Fluoride, Boron, and Boron Carbide. College of Engineering, Kansas State University, Manhattan, KS.

Shultis, J.K., McGregor, D.S., 2009. Design and performance considerations for perforated semiconductor thermal-neutron detectors. Nucl. Instrum. Methods Phys. Res. Sect. A 606 (3), 608–636.

Tsoulfanidis, N., 1995. Measurement and Detection of Radiation, 2nd ed. Taylor and Francis, Washington, DC.

Ziegler, J.F., Biersack, J.P., 2013. "SRIM-2013 Code," IBM Company.